COMMUN. MATH. SCI.
Vol. 6, No. 2, pp. 449–475
© 2008 International Press

SUPERPOSITIONS AND HIGHER ORDER GAUSSIAN BEAMS*

NICOLAY M. TANUSHEV†

Abstract. High frequency solutions to partial differential equations (PDEs) are notoriously difficult to simulate numerically due to the large number of grid points required to resolve the wave oscillations. In applications, one often must rely on approximate solution methods to describe the wave field in this regime. Gaussian beams are asymptotically valid high frequency solutions concentrated on a single curve through the domain. We show that one can form integral superpositions of such Gaussian beams to generate more general high frequency solutions to PDEs.

As a particular example, we look at high frequency solutions to the constant coefficient wave equation and construct Gaussian beam solutions with Taylor expansions of several orders. Since this PDE can be solved via a Fourier transform, we use the Fourier transform solution to gauge the error of the constructed Gaussian beam superposition solutions. Furthermore, we look at an example for which the solution exhibits a cusp caustic and investigate the order of magnitude of the wave amplitude as a function of frequency at the tip of the cusp. We show that the observed behavior is in agreement with the predictions of Maslov theory.

Key words. high frequency waves, superpositions, Gaussian beams, caustics, ray methods, wave equation, caustics

AMS subject classifications. 35L05, 41A60, 65M25

1. Introduction

Computation of high frequency waves is a necessity in many scientific applications. Fields requiring such computations include the semi-classical limit of the Schrödinger equation, communication networks, radio antenna engineering, laser optics, underwater acoustics, seismic wave propagation, and reflection seismology. These phenomena are modeled by partial differential equations (PDEs). The direct numerical integration of these PDEs is not computationally feasible, since one needs a tremendous number of grid points to resolve the rapid oscillations of the waves. As a result, one is forced to rely on approximate solutions which are valid in the high frequency regime.

Gaussian beams are approximate high frequency solutions to PDEs which are concentrated on a single ray through space-time. They derive their name from the fact that these solutions look like Gaussian distributions on planes perpendicular to the ray. The existence of such solutions has been known to the pure mathematics community since sometime in the 1960s, and these solutions have been used to obtain results on propagation of singularities in PDEs ([4] and [8]). More general solutions that are not necessarily concentrated on a single ray can be obtained from a superposition of Gaussian beams. Such superpositions have been investigated in [5], [6], and [7]. In geophysical applications, Gaussian beam superpositions have been used to model the seismic wave field [1] and for seismic migration [3]. More recently, they have been used to model the stationary-in-time atmospheric waves that result from steady airflow over topography [9].

Gaussian beams are closely related to geometric optics, also known as the WKB method or ray-tracing. In both approaches, the solution of the PDE is assumed to be

*Received: December 16, 2007; accepted (in revised version): April 2, 2008. Communicated by Olof Runborg. This work was partially supported by the National Science Foundation (UCLA VIGRE Grant No. DMS-0502315 and UT Austin RTG Grant No. DMS-0636586).

†Department of Mathematics, University of Texas at Austin, Austin, TX 78712, (nicktan@math.utexas.edu).

of the form

$$e^{ik\phi}\left[a_0+\frac{1}{k}a_1+\ldots+\frac{1}{k^N}a_N\right], \tag{1.1}$$

where k is the high frequency parameter, a_j's are the amplitude functions, and ϕ is the phase function. One then substitutes this form into the PDE to find the equations that the amplitudes and phase functions have to satisfy. Gaussian beams and geometric optics differ in the assumptions on the phase: the geometric optics method assumes that the phase is a real valued function, while the Gaussian beam construction does not.

Geometric optics has been widely used to model high frequency wave propagation in the applied mathematics community. A common problem with this method is that solving the equation for the phase using the method of characteristics leads to singularities which invalidate the approximation. Generally speaking, this breakdown occurs when nearby rays intersect, resulting in a caustic where geometric optics incorrectly predicts that the amplitude of the solution is infinite.

The geometric optics solution can be extended past caustics, once they are identified, by Maslov's method. However, caustics can occur anywhere in the domain, and their correction in numerical schemes is non-trivial. Intuitively speaking, Gaussian beams do not develop caustics, since they are concentrated on a single ray, and one ray cannot develop a caustic. Thus, a Gaussian beam is a global solution of the PDE. Mathematically, this stems from the fact that the standard symplectic form and its complexification are preserved along the flow defined by the Hessian matrix of the phase. Hence, superpositions of Gaussian beams enjoy an advantage over geometric optics in that Gaussian beam solutions are global and their superposition provides a valid approximation at caustics wherever they occur.

Each Gaussian beam is constructed from a Taylor expansion of the phase and amplitude functions. The Taylor coefficients satisfy a system of ordinary differential equations (ODEs). In numerical simulations, once the numerical computations are complete, the wave field is given by a function. To obtain the highly oscillatory solution, this function is then evaluated at each grid point of the domain. Increasing the number of points in the domain simply means that this function needs to be evaluated at more points; no additional integration of the ODEs is required. In geometric optics approaches the wave field is calculated at points along rays in the domain. To increase the number of points in the domain, one has to either add more rays (which is usually numerically too expensive) or one has to interpolate the solution. This interpolation adds an additional layer of error to the geometric optics solution.

There are some tricks to limiting the interpolation error, such as inserting additional rays only where the rays paths are diverging. However, all of these improvements are accomplished through complicated numerical procedures. Geometric optics suffers from errors in satisfying the PDE, errors in the numerical ODE integration and errors in interpolating the solution. The interpolation errors are hard to quantify since they depend on properties of the function, such as its curvature, and on the location of the points used for interpolating.

The accuracy of the Gaussian beam solution is controlled by the well-posedness theory for the PDE. Usually, these estimates state that some norm of the error is bounded by a constant (which may depend on the time t) times some appropriate norm of the error in the initial data and the error in satisfying the PDE. Thus, the

sources of error in the Gaussian beam solution are the error in approximating the initial data, errors in satisfying the PDE and errors in the numerical solution of the system of ODEs that define each beam. This gives the Gaussian beam solution a strong advantage over geometric optics, since it quantifies the error in the computed solution. Furthermore, since increasing the resolution of the solution can be accomplished without re-integration of the ODEs, one can easily examine a specific portion of the domain. In other words, the Gaussian beam solution provides an easy way to "zoom" into particular regions of the domain, which is a useful tool in applications.

In this paper we will consider Gaussian beam solutions to the constant coefficient wave equation,

$$\Box u \equiv u_{tt} - \triangle u = 0 \text{ in } \mathbb{R}_+ \times \mathbb{R}^2,$$

with u and u_t given at $t = 0$.

This problem in particular was chosen because it is easily solved using a Fourier transform. We will use this solution to benchmark the Gaussian beam solutions.

2. Convergence of Gaussian beam superpositions

Throughout this section we will use the notation

$$T_j^y[f](x)$$

to denote the j^{th}-order Taylor polynomial of f about y at the point x and

$$R_j^y[f](x)$$

to denote its remainder. That is,

$$f(x) = T_j^y[f](x) + R_j^y[f](x).$$

THEOREM 2.1. *Let $\phi_0 \in C^\infty(\mathbb{R}^n)$ be a real-valued function, $a_0 \in C_0^\infty(\mathbb{R}^n)$, and $\rho \in C_0^\infty(\mathbb{R}^n)$ be such that $\rho \geq 0$, $\rho \equiv 1$ in a ball of radius $\delta > 0$ about the origin.*

Define

$$u(x) = a_0(x) e^{ik\phi_0(x)},$$
$$v(x;y) = \left(\frac{k}{2\pi}\right)^{\frac{n}{2}} \rho(x-y) T_j^y[a_0](x) e^{ikT_{j+2}^y[\phi_0](x) - k|x-y|^2/2}.$$

Then

$$\left\| \int_{\mathbb{R}^n} v(x;y)dy - u(x) \right\|_{L^2} \leq Ck^{-\frac{j+1}{2}},$$

for some constant C.

Proof. Estimating the norm, we have

$$\begin{aligned}
&\left\| \int_{\mathbb{R}^n} v(x;y)dy - u(x) \right\|_{L^2} \\
&\leq \left\| \int_{\mathbb{R}^n} \left(\frac{k}{2\pi}\right)^{\frac{n}{2}} \rho(x-y) T_j^y[a_0](x) e^{ikT_{j+2}^y[\phi_0](x) - k|x-y|^2/2} dy - a_0(x) e^{ik\phi_0(x)} \right\|_{L^2} \\
&\leq \left\| \int_{\mathbb{R}^n} \left(\frac{k}{2\pi}\right)^{\frac{n}{2}} \rho(x-y) T_j^y[a_0](x) e^{-ikR_{j+2}^y[\phi_0](x) - k|x-y|^2/2} dy - a_0(x) \right\|_{L^2} \\
&\leq \left\| \left(\frac{k}{2\pi}\right)^{\frac{n}{2}} \int_{\mathbb{R}^n} \left[\rho(x-y) T_j^y[a_0](x) - a_0(x)\right] e^{-ikR_{j+2}^y[\phi_0](x) - k|x-y|^2/2} dy \right\|_{L^2} \\
&\qquad + \left\| \left(\frac{k}{2\pi}\right)^{\frac{n}{2}} \int_{\mathbb{R}^n} a_0(x) \left[e^{-ikR_{j+2}^y[\phi_0](x)} - 1\right] e^{-k|x-y|^2/2} dy \right\|_{L^2} \\
&:= I + J.
\end{aligned}$$

We proceed by looking at the two pieces I and J independently. Since

$$\begin{aligned}
\rho(x-y) T_j^y[a_0](x) - a_0(x) &= (\rho(x-y)-1) a_0(x) + \rho(x-y)(T_j^y[a_0](x) - a_0(x)) \\
&= (\rho(x-y)-1) a_0(x) - \rho(x-y) R_j^y[a_0](x),
\end{aligned}$$

we have:

$$\begin{aligned}
I &\leq \left\| \left(\frac{k}{2\pi}\right)^{\frac{n}{2}} \int_{\mathbb{R}^n} |(\rho(x-y)-1) a_0(x)| e^{-k|x-y|^2/2} dy \right\|_{L^2} \\
&\qquad + \left\| \left(\frac{k}{2\pi}\right)^{\frac{n}{2}} \int_{\mathbb{R}^n} |\rho(x-y) R_j^y[a_0](x)| e^{-k|x-y|^2/2} dy \right\|_{L^2} \\
&\leq \left\| \left(\frac{k}{2\pi}\right)^{\frac{n}{2}} |a_0(x)| \int_{\mathbb{R}^n} \frac{|y|^{j+1}}{\delta^{j+1}} e^{-k|y|^2/2} dy \right\|_{L^2} \\
&\qquad + \left\| \left(\frac{k}{2\pi}\right)^{\frac{n}{2}} \int_{\mathbb{R}^n} \chi(x) C |y|^{j+1} e^{-k|y|^2/2} dy \right\|_{L^2} \\
&\leq C k^{-\frac{j+1}{2}},
\end{aligned}$$

where $\chi(x) \in C_0^\infty(\mathbb{R}^n)$ such that $\chi(x) \geq 0$ and $\chi(x) \equiv 1$ for $x \in \{\mathrm{supp}(a_0) + \mathrm{supp}(\rho)\}$.

We now estimate J:

$$\begin{aligned}
J &\leq \left\| \left(\frac{k}{2\pi}\right)^{\frac{n}{2}} |a_0(x)| \int_{\mathbb{R}^n} \Big[\left|1 - \cos(kR_{j+2}^y[\phi_0](x))\right|^2 \right. \\
&\qquad \left. + \left|\sin(kR_{j+2}^y[\phi_0](x))\right|^2 \Big]^{1/2} e^{-k|x-y|^2/2} dy \right\|_{L^2} \\
&\leq \left\| \left(\frac{k}{2\pi}\right)^{\frac{n}{2}} |a_0(x)| \int_{\mathbb{R}^n} 2k |R_{j+2}^y[\phi_0](x)| e^{-k|x-y|^2/2} dy \right\|_{L^2}
\end{aligned}$$

$$\leq \left\| \left(\frac{k}{2\pi}\right)^{\frac{n}{2}} |a_0(x)| \int_{\mathbb{R}^n} 2k|y|^{j+3} e^{-k|y|^2/2} dy \right\|_{L^2}$$
$$\leq Ck^{-\frac{j+1}{2}}.$$

Thus,

$$\left\| \int_{\mathbb{R}^n} v(x;y)dy - u(x) \right\|_{L^2} \leq Ck^{-\frac{j+1}{2}}.$$

□

A result of this form also holds under much weaker assumptions on ϕ_0 and a_0:

THEOREM 2.2. *Let $\phi_0 \in C^2(\mathbb{R}^n)$ be a real-valued function and let $a_0 \in L^2(\mathbb{R}^n)$. For all $\epsilon > 0$, there exist functions a and ϕ such that for sufficiently large k,*

$$\left\| \int_{\mathbb{R}^n} v(x;y)dy - u(x) \right\|_{L^2} \leq \epsilon,$$

with

$$u(x) = a_0(x)e^{ik\phi_0(x)},$$
$$v(x;y) = \left(\frac{k}{2\pi}\right)^{\frac{n}{2}} a(y)e^{ik\phi(x;y) - k|x-y|^2/2}.$$

Before we proceed with the proof of this theorem, it is useful to record the following two lemmas.

LEMMA 2.3. *For $f \in C_0^\infty$, let*

$$f_k^*(x) = \left(\frac{k}{2\pi}\right)^{\frac{n}{2}} \int_{\mathbb{R}^n} f(y)e^{-ikR(x,y) - k|x-y|^2/2} dy,$$

with $k > 0$ and R a real-valued function. Then

$$\|f_k^*\|_{L^2} \leq \|f\|_{L^2}.$$

Proof. Note that

$$\left(\frac{k}{2\pi}\right)^{\frac{n}{2}} \int_{\mathbb{R}^n} e^{-k|x-y|^2/2} dy = 1.$$

Using the definition of f_k^* and Hölder's inequality, we have:

$$|f_k^*(x)| \leq \int \left| \left(\frac{k}{2\pi}\right)^{\frac{n}{2}} e^{-ikR(x,y) - k|x-y|^2/2} f(y) \right| dy$$
$$\leq \int \left| \left(\frac{k}{2\pi}\right)^{\frac{n}{2}} e^{-k|x-y|^2/2} f(y) \right| dy$$
$$\leq \left[\int |f(y)|^2 \left(\frac{k}{2\pi}\right)^{\frac{n}{2}} e^{-k|x-y|^2/2} dy \right]^{\frac{1}{2}} \left[\int \left(\frac{k}{2\pi}\right)^{\frac{n}{2}} e^{-k|x-y|^2/2} dy \right]^{\frac{1}{2}}$$
$$\leq \left[\int |f(y)|^2 \left(\frac{k}{2\pi}\right)^{\frac{n}{2}} e^{-k|x-y|^2/2} dy \right]^{\frac{1}{2}},$$

which implies that

$$|f_k^*(x)|^2 \leq \int |f(y)|^2 \left(\frac{k}{2\pi}\right)^{\frac{n}{2}} e^{-k|x-y|^2/2} dy.$$

After integrating over x, we have

$$\|f_k^*\|_{L^2} \leq \|f\|_{L^2}.$$

□

LEMMA 2.4. *Let $F \in C^2(\mathbb{R}^n;\mathbb{R})$. We have the following expansion for F:*

$$F(x) = F(y) + \nabla F(y)\cdot(x-y) + \frac{1}{2}(x-y)\cdot HF(y)(x-y) + R(x,y),$$

where $HF(y)$ denotes the Hessian matrix of F at y and

$$R(x,y) = (x-y)\cdot\left[\int_0^1 (1-t)[HF(tx+(1-t)y) - HF(y)]dt\right](x-y).$$

Proof. The proof of this lemma follows from the Fundamental Theorem of Calculus and integration by parts. We omit the proof for brevity. □

Proof. (Theorem 2.2) By Lem. 2.4 we have the following expansion for $\phi_0(x)$:

$$\phi_0(x) = \phi_0(y) + \nabla\phi_0(y)\cdot(x-y) + \frac{1}{2}(x-y)\cdot H\phi_0(y)(x-y) + R(x,y),$$

with $H\phi_0(y)$ and $R(x,y)$ as defined in the Lemma.

Now choose $a \in C_0^\infty(\mathbb{R}^n)$, such that $\|a_0 - a\|_{L^2} < \epsilon/2$, and define

$$\phi(x;y) = \phi_0(y) + \nabla\phi_0(y)\cdot(x-y) + \frac{1}{2}(x-y)\cdot H\phi_0(y)(x-y)$$

and

$$v(x;y) = \left(\frac{k}{2\pi}\right)^{\frac{n}{2}} a(y) e^{ik\phi(x;y) - k|x-y|^2/2}.$$

We now estimate

$$\begin{aligned}
&\left\| u(x) - \int_{\mathbb{R}^n} v(x;y)dy \right\|_{L^2} \\
&= \left\| a_0(x)e^{ik\phi_0(x)} - \left(\frac{k}{2\pi}\right)^{\frac{n}{2}} \int_{R^n} a(y) e^{ik\phi(x;y) - k|x-y|^2/2} dy \right\|_{L^2} \\
&= \left\| e^{ik\phi_0(x)} \left[a_0(x) - \left(\frac{k}{2\pi}\right)^{\frac{n}{2}} \int_{\mathbb{R}^n} a(y) e^{-ikR(x,y) - k|x-y|^2/2} dy \right] \right\|_{L^2} \\
&\equiv \|a_0(x) - a_k^*(x)\|_{L^2} \\
&\leq \|a_0(x) - a(x)\|_{L^2} + \|a(x) - a_k^*(x)\|_{L^2} \\
&\leq \epsilon/2 + \|a(x) - a_k^*(x)\|_{L^2}.
\end{aligned}$$

Thus, we need to verify that $\|a-a_k^*\|_{L^2}\leq\epsilon/2$ as $k\to\infty$. First, we verify this over a compact domain Ω:

$$\begin{aligned}\|a-a_k^*\|_{L^2,\Omega}^2&=\int_\Omega\left|a(x)-\left(\frac{k}{2\pi}\right)^{\frac{n}{2}}\int_{\mathbb{R}^n}a(y)e^{-ikR(x,y)-k|x-y|^2/2}dy\right|^2dx\\&=\int_\Omega\left|\left(\frac{k}{2\pi}\right)^{\frac{n}{2}}\int_{R^n}\left[a(x)-a(y)e^{-ikR(x,y)}\right]e^{-k|x-y|^2/2}dy\right|^2dx.\end{aligned}$$

Continuing the estimate, by Hölder's inequality, we have

$$\begin{aligned}\|a-a_k^*\|_{L^2,\Omega}^2&\leq\left(\frac{k}{2\pi}\right)^{\frac{n}{2}}\int_\Omega\int_{R^n}\left|a(x)-a(y)e^{-ikR(x,y)}\right|^2e^{-k|x-y|^2/2}dydx\\&\leq\ 2\left(\frac{k}{2\pi}\right)^{\frac{n}{2}}\int_\Omega\int_{R^n}\left[|a(x)-a(y)|^2+\left|a(y)\left(1-e^{-ikR(x,y)}\right)\right|^2\right]e^{-k|x-y|^2/2}dydx,\end{aligned}$$

and letting $(x-y)=z/k^{1/2}$ and eliminating y, we get

$$\begin{aligned}\|a-a_k^*\|_{L^2,\Omega}^2\leq\ &2\left(\frac{1}{2\pi}\right)^{\frac{n}{2}}\int_\Omega\int_{R^n}\left|a(x)-a(x-z/k^{1/2})\right|^2e^{-|z|^2/2}dzdx\\&+\ 2\left(\frac{1}{2\pi}\right)^{\frac{n}{2}}\int_\Omega\int_{R^n}\left|a(x-z/k^{1/2})\left(1-e^{-ikR(x,x-z/k^{1/2})}\right)\right|^2e^{-|z|^2/2}dzdx\\:=\ &I+J\end{aligned}$$

Let $D=\mathrm{supp}(a)$. Since a is compactly supported and smooth,

- the measure of D is finite, $\mu(D)<\infty$,
- $|a(x)|<M$, for some $M>0$, and
- a is globally Lipschitz, $|a(x)-a(x-z/k^{1/2})|\leq L|z|/k^{1/2}$.

Estimating I and J independently, we have

$$\begin{aligned}I=\ &2\left(\frac{1}{2\pi}\right)^{\frac{n}{2}}\int_\Omega\int_{\mathbb{R}^n}\left|a(x)-a(x-z/k^{1/2})\right|^2e^{-|z|^2/2}dzdx\\\leq\ &2\left(\frac{1}{2\pi}\right)^{\frac{n}{2}}\int_\Omega\int_{\mathbb{R}^n}\frac{L^2|z|^2}{k}e^{-|z|^2/2}dzdx\\\leq\ &2L^2\mu(\Omega)\left(\frac{1}{2\pi}\right)^{\frac{n}{2}}\int_{\mathbb{R}^n}\frac{|z|^2}{k}e^{-|z|^2/2}dz\\\leq\ &\epsilon^2/32\quad\text{for large enough}\quad k\end{aligned}$$

We take a minute to estimate the remainder, $-ikR(x,x-\frac{z}{k^{1/2}})$, for large k. Let r be large enough, so that

$$8M^2\mu(\Omega)\left(\frac{1}{2\pi}\right)^{\frac{n}{2}}\int_{|z|>r}e^{-|z|^2/2}dz\leq\epsilon^2/64.$$

Then

$$\begin{aligned}&-ik\frac{z}{k^{1/2}}\cdot\left[\int_0^1(1-t)\left[H\phi_0(tx+(1-t)(x-\frac{z}{k^{1/2}}))-H\phi_0(x-\frac{z}{k^{1/2}})\right]dt\right]\frac{z}{k^{1/2}}\\=&-iz\cdot\left[\int_0^1(1-t)\left[H\phi_0(x+(t-1)\frac{z}{k^{1/2}})-H\phi_0(x-\frac{z}{k^{1/2}})\right]dt\right]z.\end{aligned}$$

Since $H\phi_0$ is continuous, it is uniformly continuous over compact sets in (x,z). Thus, for $|z|\le r$ and every $\delta>0$, for sufficiently large k, we have that

$$|-ikR(x,x-z/k^{1/2})|<\delta.$$

Thus for small enough δ, we have the following estimate for J:

$$\begin{aligned}
J\le\ & 2\left(\frac{1}{2\pi}\right)^{\frac{n}{2}}\int_\Omega\int_{|z|\le r}\left|a(x-z/k^{1/2})(1-e^{-ikR(x,x-z/k^{1/2})})\right|^2 e^{-|z|^2/2}dzdx\\
&+\ 8M^2\left(\frac{1}{2\pi}\right)^{\frac{n}{2}}\int_\Omega\int_{|z|>r}e^{-|z|^2/2}dzdx\\
\le\ & 2\left(\frac{1}{2\pi}\right)^{\frac{n}{2}}M^2\mu(\Omega)\mu(\{z:|z|\le r\})(|1-\cos(\delta)|^2+|\sin(\delta)|^2)+\epsilon^2/64\\
\le\ & \epsilon^2/32.
\end{aligned}$$

Putting all of these estimates together, we see that

$$\begin{aligned}
\|a-a_k^*\|_{L^2,\Omega}^2 &\le \epsilon^2/32+\epsilon^2/32\\
&\le \epsilon^2/16
\end{aligned}$$

and

$$\begin{aligned}
\|a-a_k^*\|_{L^2} &= \|a-a_k^*\|_{L^2,D}+\|a-a_k^*\|_{L^2,D^c}\\
&\le \epsilon/4+\|a_k^*\|_{L^2,D^c}\\
&\le \epsilon/4+\|a_k^*\|_{L^2}-\|a_k^*\|_{L^2,D}\\
&\le \epsilon/4+\|a\|_{L^2}-\|a_k^*\|_{L^2,D}\\
&\le \epsilon/4+\|a\|_{L^2,D}-\|a_k^*\|_{L^2,D}\\
&\le \epsilon/4+\|a-a_k^*\|_{L^2,D}\\
&\le \epsilon/4+\epsilon/4\\
&\le \epsilon/2,
\end{aligned}$$

where we have used Lem. 2.3. Thus, for large enough k,

$$\begin{aligned}
\left\|u(x)-\int_{\mathbb{R}^n}v(x;y)dy\right\|_2 &\le \epsilon/2+\|a(x)-a_k^*(x)\|_{L^2}\\
&\le \epsilon,
\end{aligned}$$

which proves the result. ∎

3. Constant coefficient wave equation

In this section, we investigate Gaussian beam solutions to the constant-coefficient wave equation,

$$\begin{aligned}
\Box u\equiv u_{tt}-\triangle u=0\ \text{ in }\ \mathbb{R}_+\times\mathbb{R}^2,\\
u=f(x)\ \text{ for } t=0,\\
u_t=g(x)\ \text{ for } t=0.
\end{aligned}\tag{3.1}$$

This problem was chosen in particular because it is easily solved using a Fourier transform. The solution of the initial value problem can be immediately written in

terms of the Fourier transform in the space variables x of the initial data (η is the dual variable):

$$u_F = \frac{1}{2}\mathcal{F}^{-1}\left\{\mathcal{F}\{f\}\left(e^{i|\eta|t}+e^{-i|\eta|t}\right)+\frac{\mathcal{F}\{g\}}{i|\eta|}\left(e^{i|\eta|t}-e^{-i|\eta|t}\right)\right\}.$$

We will use the Fourier Transform solution to benchmark the Gaussian beam solutions.

The wave equation (3.1) is well-posed, and we have the following estimate for the solution.

THEOREM 3.1. *Let u satisfy*

$$\begin{aligned} u_{tt}-\triangle u = F(t,x) \quad &in \ \ [0,T]\times\mathbb{R}^n,\\ u = f(x) \quad &for\ t=0,\\ u_t = g(x) \quad &for\ t=0, \end{aligned}$$

with F, f and g compactly supported. Then

$$\left[\|\nabla u\|^2_{L^2(\mathbb{R}^n)}+\|\partial_t u\|^2_{L^2(\mathbb{R}^n)}\right]^{\frac{1}{2}} \le \left[\|f\|^2_{H^1(\mathbb{R}^n)}+\|g\|^2_{L^2(\mathbb{R}^n)}\right]^{\frac{1}{2}} + T\sup_{t\in[0,T]}\|F(t,\cdot)\|_{L^2(\mathbb{R}^n)}$$

for $t\in[0,T]$.

Proof. This result can be obtained by differentiating the energy $\|\nabla u\|^2_{L^2(\mathbb{R}^n)}+\|u_t\|^2_{L^2(\mathbb{R}^n)}$ in t. ∎

3.1. Gaussian beam solutions.

Phase and Amplitude Equations. Upon substituting the ansatz

$$u = e^{ik\phi}\left[a+\frac{1}{k}b\right] \tag{3.2}$$

into

$$u_{tt}-\triangle u = 0 \tag{3.3}$$

and collecting powers of the large parameter, k, we obtain the following equations for the phase and amplitudes:

$$\begin{aligned} k^2 &: (-\phi_t^2+\phi_{x_1}^2+\phi_{x_2}^2)a \ = \ 0,\\ k^1 &: 2i(\phi_t a_t-\phi_{x_1}a_{x_1}-\phi_{x_2}a_{x_2})+i(\phi_{tt}-\phi_{x_1x_1}-\phi_{x_2x_2})a+(-\phi_t^2+\phi_{x_1}^2+\phi_{x_2}^2)b \ = \ 0,\\ k^0 &: 2i(\phi_t b_t-\phi_{x_1}b_{x_1}-\phi_{x_2}b_{x_2})+i(\phi_{tt}-\phi_{x_1x_1}-\phi_{x_2x_2})b+(a_{tt}-a_{x_1x_1}-a_{x_2x_2}) \ = \ 0. \end{aligned}$$

These equations simplify to:

$$\begin{aligned} 2(\phi_t\phi_t-\phi_{x_1}\phi_{x_1}-\phi_{x_2}\phi_{x_2}) &= 0,\\ 2(\phi_t a_t-\phi_{x_1}a_{x_1}-\phi_{x_2}a_{x_2}) &= -a\Box\phi,\\ 2(\phi_t b_t-\phi_{x_1}b_{x_1}-\phi_{x_2}b_{x_2}) &= i\Box a-b\Box\phi. \end{aligned} \tag{3.4}$$

The first equation is called the eikonal equation, and the others are referred to as the transport equations. In the spirit of the Gaussian beam construction (see Appendix A.1 of [9], or Section 2.1 of [8]), we will not look for global solutions of these equations.

Instead, we will solve them on a single characteristic originating from a point $y=(y_1,y_2)$ on the initial data surface $t=0$. Thus, we will view these equations as ODEs along the characteristic. In order to solve these ODEs for the phase, the amplitudes and their derivatives, we need initial conditions. We can find the initial conditions from the initial data for the PDE and the eikonal and transport equations, since they hold for all x on $t=0$. With

$$u|_{t=0}=f=\left[A(x)+\frac{1}{k}B(x)\right]e^{ik\Phi(x)},$$
$$u_t|_{t=0}=g=[kC(x)+D(x)]e^{ik\Phi(x)}$$

at $t=0$,

$$\begin{array}{ccc}\phi=\Phi, & \phi_x=\nabla_x\Phi, & \phi_t=\Phi_t^{\pm}\equiv\pm\sqrt{|\nabla_x\Phi|},\\ a^+ + a^- = A, & i\Phi_t^+ a^+ + i\Phi_t^- a^- = C, & a_t^{\pm}=\frac{2\nabla_x\Phi\cdot\nabla_x a^{\pm}-a^{\pm}\Box\Phi}{2\Phi_t^{\pm}},\end{array} \tag{3.5}$$

and so on. The "±" gives us two waves, one propagating in one direction and the other propagating in the opposite direction. For the remainder of the paper, we will assume that the initial data for the PDE is chosen to give one-way propagating waves and we will drop the "±" notation, so

$$\begin{array}{lll}\phi=\Phi, & \phi_x=\nabla_x\Phi, & \phi_t=\Phi_t\equiv\sqrt{|\nabla_x\Phi|},\\ a=A, & & a_t=\frac{2\nabla_x\Phi\cdot\nabla_x A-A\Box\Phi}{2\Phi_t},\end{array} \tag{3.6}$$

and

$$u_t|_{t=0}=g=\left[k\Phi_t\left(A+\frac{1}{k}B\right)+A_t+\frac{1}{k}B_t\right]e^{ik\Phi(x)}.$$

Once the ODEs have been solved, we have the phase and amplitudes along with their derivatives on the characteristic. We extend them away from the characteristic through a Taylor expansion and a localizing cut-off function.

The accuracy of the Gaussian beam superposition solution depends on the accuracy of the individual beams. Two factors that control this accuracy are

- the number of terms in the Taylor expansions for the phase and amplitudes,
- the number of terms in the ansatz (1.1).

These two factors are not independent. As can be seen in the construction of Gaussian beams, the Taylor coefficients of each one of the amplitudes in the ansatz (1.1) depends on the coefficients of the previous amplitudes and the phase. In other words, we can't define arbitrarily many Taylor coefficients for the a_j amplitude without a certain number of the coefficients of the a_l amplitudes for $l=0,\ldots,(j-1)$ and of the phase ϕ. On the other hand, while we can define the Taylor coefficients of the phase without any of the amplitude coefficients, taking many coefficients is unnecessary, since eventually their overall effect on the accuracy of the Gaussian beam solution is smaller than that of amplitudes that have been omitted by truncating the asymptotic expansion of the ansatz (1.1) at N. We keep these two competing factors in mind when defining the higher order Gaussian beams in the next several sections.

First Order Gaussian Beam Solution To obtain a Gaussian Beam solution, as a bare minimum, we must take terms up to 2^{nd} order for ϕ and up to 0^{th} order for the first amplitude function a in their respective Taylor expansions. We refer to this as a

"first" order Gaussian beam. The equations for the characteristic $(\mathcal{T},\mathcal{X})$ originating from y at $t=0$ are

$$\begin{aligned} \dot{\mathcal{T}} &= 2\tau, & \mathcal{T}(0) &= 0, \\ \dot{\mathcal{X}} &= -2\xi, & \mathcal{X}(0) &= y=(y_1,y_2), \\ \dot{\tau} &= 0, & \tau(0) &= \Phi_t(y), \\ \dot{\xi} &= 0, & \xi(0) &= \nabla_y\Phi(y), \end{aligned} \tag{3.7}$$

where $\dot{}$ signifies differentiation with respect to the ray parameter s. Also, recall that $\tau=\phi_t$ and $\xi=\nabla_x\phi$.

Proceeding, we get an equation for ϕ,

$$\dot{\phi}=0, \quad \phi(0)=\Phi(y), \tag{3.8}$$

and its second derivatives,

$$\dot{\phi}_{\alpha\beta}=-2\phi_{t\alpha}\phi_{t\beta}+2\phi_{x_1\alpha}\phi_{x_1\beta}+2\phi_{x_2\alpha}\phi_{x_2\beta},$$

where α and β stand for any one of t, x_1 or x_2. The initial conditions are

$$(\phi_{\alpha\beta})=\begin{pmatrix} * & * & * \\ * & \Phi_{x_1x_1}+i & \Phi_{x_1x_2} \\ * & \Phi_{x_1x_2} & \Phi_{x_2x_2}+i \end{pmatrix},$$

where the $*$'s are chosen so that

$$\begin{gathered} \phi_{\alpha\beta}=\phi_{\beta\alpha}, \\ 0=\dot{\phi}_\alpha=2\phi_t\phi_{t\alpha}-2\phi_{x_1}\phi_{x_1\alpha}-2\phi_{x_2}\phi_{x_2\alpha}. \end{gathered}$$

The $+i$ term is added to give the initial data a Gaussian beam profile.

Note that the equations for the second derivatives of ϕ are nonlinear. One can rewrite them as a nonlinear Ricatti matrix equation. Even though this matrix equation is also nonlinear, for the initial condition that we have chosen, there exists a global solution. One shows this by rewriting the Ricatti equations in terms of two linear matrix equations (see Appendix A.1 of [9], or Section 2.1 of [8]). Although one can use these two linear equations to compute the second derivatives of ϕ, it is more advantageous in simulations to integrate the nonlinear version of the equations, since there are fewer equations and there is no need to invert a matrix.

Finally, we have the transport equation,

$$\dot{a}=-a\Box\phi, \quad a(0)=A(y).$$

Second Order Gaussian Beam Solution. A "second" order Gaussian beam has terms up to 3^{rd} order for the phase and up to 1^{st} order for the first amplitude a. As before, we obtain equations for these quantities by differentiating the eikonal and transport equations (again, α, β and γ can be any one of t, x_1 or x_2):

$$\begin{aligned} \dot{\phi}_{\alpha\beta\gamma} = &-2\phi_{t\gamma}\phi_{t\alpha\beta}+2\phi_{x_1\gamma}\phi_{x_1\alpha\beta}+2\phi_{x_2\gamma}\phi_{x_2\alpha\beta} \\ &+\partial_\gamma\left(-2\phi_{t\alpha}\phi_{t\beta}+2\phi_{x_1\alpha}\phi_{x_1\beta}+2\phi_{x_2\alpha}\phi_{x_2\beta}\right). \end{aligned}$$

The initial conditions for these equations come from the relations given by the derivatives of the eikonal equation on the initial surface $t=0$. One must remember to include the $+i$ imaginary part in the appropriate second derivatives. This imaginary

part carries through in the initial conditions for the third and higher derivatives of the phase.

The equations for the derivatives of the first amplitude are

$$\dot{a}_\alpha = -2a_t\phi_{t\alpha} + 2a_{x_1}\phi_{x_1\alpha} + 2a_{x_2}\phi_{x_2\alpha} + \partial_\alpha(-a\Box\phi).$$

The initial conditions are obtained from the relations given by the derivatives of the first amplitude equation on $t=0$.

Third Order Gaussian Beam Solution. A "third" order Gaussian beam has terms up to 4^{th} order for the phase, up to 2^{nd} order for the first amplitude a, and up to 0^{th} order for the second amplitude b. The equations are as follows (α, β, γ and δ can be any one of t, x_1 or x_2):

$$\begin{aligned}\dot{\phi}_{\alpha\beta\gamma\delta} = &-2\phi_{t\delta}\phi_{t\alpha\beta\gamma} + 2\phi_{x_1\delta}\phi_{x_1\alpha\beta\gamma} + 2\phi_{x_2\delta}\phi_{x_2\alpha\beta\gamma}\\ &+\partial_\delta\left(-2\phi_{t\gamma}\phi_{t\alpha\beta} + 2\phi_{x_1\gamma}\phi_{x_1\alpha\beta} + 2\phi_{x_2\gamma}\phi_{x_2\alpha\beta}\right)\\ &+\partial_{\delta\gamma}\left(-2\phi_{t\alpha}\phi_{t\beta} + 2\phi_{x_1\alpha}\phi_{x_1\beta} + 2\phi_{x_2\alpha}\phi_{x_2\beta}\right),\end{aligned}$$

$$\begin{aligned}\dot{a}_{\alpha\beta} = &-2a_{t\alpha}\phi_{t\beta} + 2a_{x_1\alpha}\phi_{x_1\beta} + 2a_{x_2\alpha}\phi_{x_2\beta}\\ &+\partial_\beta\left(-2a_t\phi_{t\alpha} + 2a_{x_1}\phi_{x_1\alpha} + 2a_{x_2}\phi_{x_2\alpha}\right)\\ &+\partial_{\alpha\beta}(-a\Box\phi),\end{aligned}$$

$$\dot{b} = i\Box a - b\Box\phi.$$

The initial conditions are obtained as in the case of second order Gaussian beams.

Superpositions. After the equations for the various phase and amplitude Taylor coefficients have been solved, we know the characteristic path, $(\mathcal{T}(s;y),\mathcal{X}(s;y))$, that originates from $(0,y_1,y_2)$. Evaluating all of the Taylor coefficients and paths for s so that $\mathcal{T}(s;y)=t$, we can define the following Gaussian beams:

$$\begin{aligned}v_1(t,x;y) &= \rho(x-\mathcal{X})\left[T_0^{\mathcal{X}}[a](x)\right]e^{ikT_2^{\mathcal{X}}[\phi](x)},\\ v_2(t,x;y) &= \rho(x-\mathcal{X})\left[T_1^{\mathcal{X}}[a](x)\right]e^{ikT_3^{\mathcal{X}}[\phi](x)},\\ v_3(t,x;y) &= \rho(x-\mathcal{X})\left[T_2^{\mathcal{X}}[a](x) + \frac{1}{k}T_0^{\mathcal{X}}[b](x)\right]e^{ikT_4^{\mathcal{X}}[\phi](x)},\end{aligned}$$

where $T_j^Y[f](z)$ is the j^{th} order Taylor polynomial of f about Y evaluated at z, and ρ is a cut-off function such that on its support the Taylor expansion of ϕ has a positive imaginary part. We form the superpositions

$$u_j(t,x) = \frac{k}{2\pi}\int_{\text{supp}\{f\}} v_j(t,x;y)dy \tag{3.9}$$

for $j=1,2,3$. As the v_j's are asymptotic solutions of the wave equation, so will be their superpositions u_j. All that remains to be checked is that these superpositions accurately approximate the initial data. Evaluating at $t=0$, we find that

$$\begin{aligned}v_1(0,x;y) &= \rho(x-y)e^{ikT_2^y[\Phi](x)-k|x-y|^2/2}(T_0^y[A](x)),\\ v_2(0,x;y) &= \rho(x-y)e^{ikT_3^y[\Phi](x)-k|x-y|^2/2}(T_1^y[A](x)),\\ v_3(0,x;y) &= \rho(x-y)e^{ikT_4^y[\Phi](x)-k|x-y|^2/2}\left(T_2^y[A](x) + \frac{1}{k}T_0^y[B](x)\right).\end{aligned}$$

Note that differentiating these expressions in x will either introduce a factor of k or lower the order of the Taylor expansion for the amplitude by 1. Differentiating ρ yields an expression which vanishes in a neighborhood of y, so this term is smaller than any inverse power of k in the superposition as $k\to\infty$. Thus, by applying Theorem 2.1, we have

$$\begin{aligned}\|u_1|_{t=0}-f\|_{H^1}&\le Ck^{-1/2+1},\\ \|u_2|_{t=0}-f\|_{H^1}&\le Ck^{-1+1},\\ \|u_3|_{t=0}-f\|_{H^1}&\le Ck^{-3/2+1}.\end{aligned}$$

We also need to look at the initial data for the time derivative of the solution. We compute that

$$\begin{aligned}\partial_t v_1(t,x;y)=\frac{ds}{dt}\Big[&ik\rho(x-\mathcal{X})T_0^{\mathcal{X}}[a](x)\left(T_2^{\mathcal{X}}[\dot\phi](x)-\dot{\mathcal{X}}_jT_1^{\mathcal{X}}[\phi_{x_j}](x)\right)\\ &-\dot{\mathcal{X}}_j\rho_{x_j}(x-\mathcal{X})T_0^{\mathcal{X}}[a](x)+\rho(x-\mathcal{X})T_0^{\mathcal{X}}[\dot a](x)\Big]e^{ikT_2^{\mathcal{X}}[\phi](x)}.\end{aligned}$$

Recognizing that

$$\frac{ds}{dt}\left(T_j^{\mathcal{X}}[\dot f](x)-\dot{\mathcal{X}}_lT_{j-1}^{\mathcal{X}}[f_{x_l}](x)\right)=T_{j-1}^{\mathcal{X}}[f_t](x)+E_j,$$

where E_j is a remainder term that is $O(|x-\mathcal{X}|^j)$ and evaluating at $t=0$, we have

$$\partial_t v_1(0,x;y)=\Big[ik\rho(x-y)T_0^y[A](x)T_1^y[\Phi_t](x)+O(k|x-y|^2+1)\Big]e^{ikT_2^y[\Phi](x)-k|x-y|^2/2}.$$

Similarly, we compute that

$$\begin{aligned}\partial_t v_2(t,x;y)=\frac{ds}{dt}\Big[&ik\rho(x-\mathcal{X})T_1^{\mathcal{X}}[a](x)\left(T_3^{\mathcal{X}}[\dot\phi](x)-\dot{\mathcal{X}}_jT_2^{\mathcal{X}}[\phi_{x_j}](x)\right)\\ &+\rho(x-\mathcal{X})\left(T_1^{\mathcal{X}}[\dot a](x)-\dot{\mathcal{X}}_jT_0^{\mathcal{X}}[a_{x_j}](x)\right)\\ &-\dot{\mathcal{X}}_j\rho_{x_j}(x-\mathcal{X})T_1^{\mathcal{X}}[a](x)\Big]e^{ikT_3^{\mathcal{X}}[\phi](x)}\end{aligned}$$

and

$$\begin{aligned}\partial_t v_3(t,x;y)=\frac{ds}{dt}\Big[\quad&ik\rho(x-\mathcal{X})\left(T_2^{\mathcal{X}}[a](x)+\frac{1}{k}T_0^{\mathcal{X}}[b](x)\right)\left(T_4^{\mathcal{X}}[\dot\phi](x)-\dot{\mathcal{X}}_jT_3^{\mathcal{X}}[\phi_{x_j}](x)\right)\\ &+\rho(x-\mathcal{X})\left(T_2^{\mathcal{X}}[\dot a](x)-\dot{\mathcal{X}}_jT_1^{\mathcal{X}}[a_{x_j}](x)\right)+\frac{1}{k}\rho(x-\mathcal{X})T_0^{\mathcal{X}}[\dot b](x)\\ &-\dot{\mathcal{X}}_j\rho_{x_j}(x-\mathcal{X})\left(T_2^{\mathcal{X}}[a](x)+\frac{1}{k}T_0^{\mathcal{X}}[b](x)\right)\Big]e^{ikT_4^{\mathcal{X}}[\phi](x)}.\end{aligned}$$

Again, substituting and evaluating at $t=0$, we have

$$\begin{aligned}\partial_t v_2(0,x;y)=\big[&ik\rho(x-y)T_1^y[A](x)T_2^y[\Phi_t](x)+O(k|x-y|^3)\\ &+\rho(x-y)T_0^y[A_t](x)+O(|x-y|)\\ &+O(|x-y|^\infty)\big]e^{ikT_3^y[\Phi](x)-k|x-y|^2/2}\end{aligned}$$

and

$$\partial_t v_3(0,x;y) = \Bigg[ik\rho(x-y)\left(T_2^y[A](x)+\frac{1}{k}T_0^y[B](x)\right)\left(T_3^y[\Phi_t](x)+O(|x-y|^4)\right) + \rho(x-y)T_1^y[A_t](x)+O(|x-y|^2+k^{-1}) + O(|x-y|^\infty)\Bigg] e^{ikT_4^y[\Phi](x)-k|x-y|^2/2}.$$

Thus, by applying Theorem 2.1 and using the ideas of its proof, we have that

$$\begin{aligned} \|\partial_t u_1|_{t=0} - g\|_{L^2} &\le Ck^{1/2}, \\ \|\partial_t u_2|_{t=0} - g\|_{L^2} &\le Ck^{0}, \\ \|\partial_t u_3|_{t=0} - g\|_{L^2} &\le Ck^{-1/2}. \end{aligned}$$

Finally, we look at $F_j = \Box u_j$ in the $L^2(\mathbb{R}^2)$ norm. We have

$$\begin{aligned} \|F_j(t,\cdot)\|_{L^2}^2 &= \int_{\mathbb{R}^2}\left|\int_{\mathrm{supp}\{f\}} \Box u_j dy\right|^2 dx \\ &= \int_{\mathbb{R}^2}\left|\int_{\mathrm{supp}\{f\}} k\sum_{l=-2}^{N-2} c_l^j k^{-l} e^{ik\phi} dy\right|^2 dx, \end{aligned}$$

where N is the number of terms in asymptotic expansion (1.1), i.e., $N=1$ for 1st and 2nd order beams and $N=2$ for 3rd order beams. By the construction of Gaussian beams, each c_l^j vanishes to order $j-2l-3$ on the characteristic and is independent of k, as these c_l^j's were used to define the eikonal and transport equations (3.4).

Now, estimating this integral,

$$\begin{aligned} &\int_{\mathbb{R}^2}\left|\int_{\mathrm{supp}\{f\}} k\sum_{l=-2}^{N-2} c_l^j k^{-l} e^{ik\phi} dy\right|^2 dx \\ &\qquad \le \mu(\mathrm{supp}\{f\})\int_{\mathrm{supp}\{f\}}\int_{\mathbb{R}^2}\left|k\sum_{l=-2}^{N-2} c_l^j k^{-l}\right|^2 e^{-2k\mathrm{Im}[\phi]} dxdy. \end{aligned}$$

We estimate the contribution of each beam, as in Lem. 2.8 in [8], by introducing ray-centered and $k^{-1/2}$ rescaled coordinates, z. Note that on $t\in[0,T]$, there is a positive function $\alpha(y)$ such that $k\mathrm{Im}[\phi] \ge \alpha(y)|z|^2$ and thus we have that

$$\begin{aligned} &\|F_j(t,\cdot)\|_{L^2}^2 \\ &\le C\sum_{l,s=-2}^{N-2}\int_{\mathrm{supp}\{f\}}\int_{\mathbb{R}^2} k^{2-l-s}\left|c_l^j(t,k^{-1/2}z,y)c_s^j(t,k^{-1/2}z,y)\right| e^{-\alpha(y)|z|^2} k^{-1} dzdy. \end{aligned}$$

As $c_l^j c_s^j$ vanishes to $2(j-l-s-3)$ on the characteristic,

$$k^{j-l-s-2}\left|c_l^j(t,k^{-1/2}z,y)c_s^j(t,k^{-1/2}z,y)\right|$$

is bounded as $k\to\infty$. Hence

$$\|F_j(t,\cdot)\|_{L^2}^2 \leq \int_{\text{supp}\{f\}} C_T(y) k^{-j+3} dy,$$

where $C_T(y)$ is a continuous function, since the Gaussian beams depend continuously on y. Thus,

$$\|F_j(t,\cdot)\|_{L^2} \leq C_T k^{\frac{-j+3}{2}},$$

which immediately gives us

$$\begin{aligned}
\|F_1(t,\cdot)\|_{L^2} &\leq C_T k^1,\\
\|F_2(t,\cdot)\|_{L^2} &\leq C_T k^{1/2},\\
\|F_3(t,\cdot)\|_{L^2} &\leq C_T k^0.
\end{aligned}$$

We note that this estimate is not sharp. For example, in the case of no caustics, one can improve this estimate by k^{-1}. It seems that one can also improve this estimate when caustics are present.

Putting all of these estimates together, we have the estimates

$$\begin{aligned}
\left[\|\nabla(u_1-u)\|_{L^2}^2 + \|\partial_t(u_t-u_1)\|_{L^2}^2\right]^{\frac{1}{2}} &\leq C_T(k^{1/2}+Tk^1),\\
\left[\|\nabla(u_2-u)\|_{L^2}^2 + \|\partial_t(u_t-u_2)\|_{L^2}^2\right]^{\frac{1}{2}} &\leq C_T(k^0+Tk^{1/2}),\\
\left[\|\nabla(u_3-u)\|_{L^2}^2 + \|\partial_t(u_t-u_3)\|_{L^2}^2\right]^{\frac{1}{2}} &\leq C_T(k^{-1/2}+Tk^0).
\end{aligned}$$

It appears that the first three orders of Gaussian beam superpositions do not converge as $k \to \infty$. However, there are two things that one must keep in mind. First, the estimate on F_j is not sharp, and second, the energy in the initial data is on the order of k. If one were to rescale this energy to be of order 1 and improve the estimate on F by any small amount, all three superposition solutions will converge as k goes to infinity.

3.2. Simple example of an initial value problem: traveling waves. We choose the initial data for the PDE (3.1) to be

$$f = u|_{t=0} = e^{ik\Phi(x)}\left[A(x) + \frac{1}{k}B(x)\right],$$

where

$$\begin{aligned}
\Phi(x) &= x^5 + y^5 + x^3 + y^3 + x + y,\\
A(x) &= \sin(x),\\
B(x) &= 0,
\end{aligned}$$

and

$$g = u_t|_{t=0} = e^{ik\Phi}\left[ik\Phi_t\left(A + \frac{1}{k}B\right) + A_t + \frac{1}{k}B_t\right],$$

where Φ_t, A_t and B_t are determined by the equations in Section 3.1 to give waves that propagate in only one direction (i.e., with positive square root in Equation (3.5)). We also fix the high frequency parameter $k = 200$.

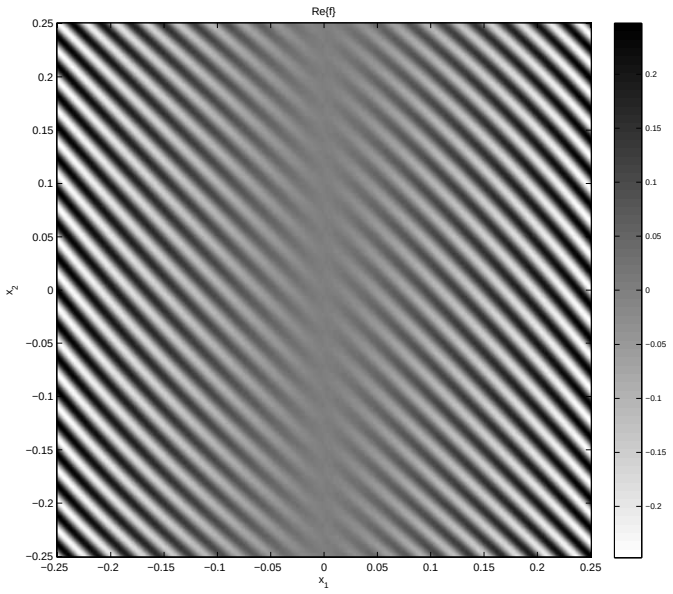

FIG. 3.1. *Initial data for the wave equation: Traveling Waves*

Comparisons. The numerical calculations of the Fourier transform solution and the Gaussian beam superpositions were carried out using a combination of Matlab and C. The Fourier transform solution will be used as the "true" solution to find the error in the wave field that is present in the Gaussian beam superpositions. For 2^{nd} and 3^{rd} order beams, the required cut-off function ρ is obtained by mollifying the characteristic function of the set where the quadratic imaginary part of the phase is twice the rest of the imaginary part.

Figure 3.2 shows the absolute value of the difference between the Fourier transform solution and the Gaussian beam superpositions along $x_2 = 0$ at $t = 0$, while Figure 3.3 shows the same difference at $t = 0.2$. The numerically computed norms of the differences are given in Table 3.1. As suggested by Theorem 2.1, the approximation of the initial data improves significantly with the addition of more terms in the Taylor expansions.

	Difference at $t=0$		Difference at $t=0.2$	
	L_2-norm	H_1-norm	L_2-norm	H_1-norm
1^{st} order	0.011102	3.4491	0.017991	6.5349
2^{nd} order	0.0012565	0.39494	0.0029652	1.0969
3^{rd} order	7.9522×10^{-6}	0.0024564	0.00027218	0.098785

TABLE 3.1. *Norm differences between the Fourier transform solution and the Gaussian beam superpositions for the traveling waves example.*

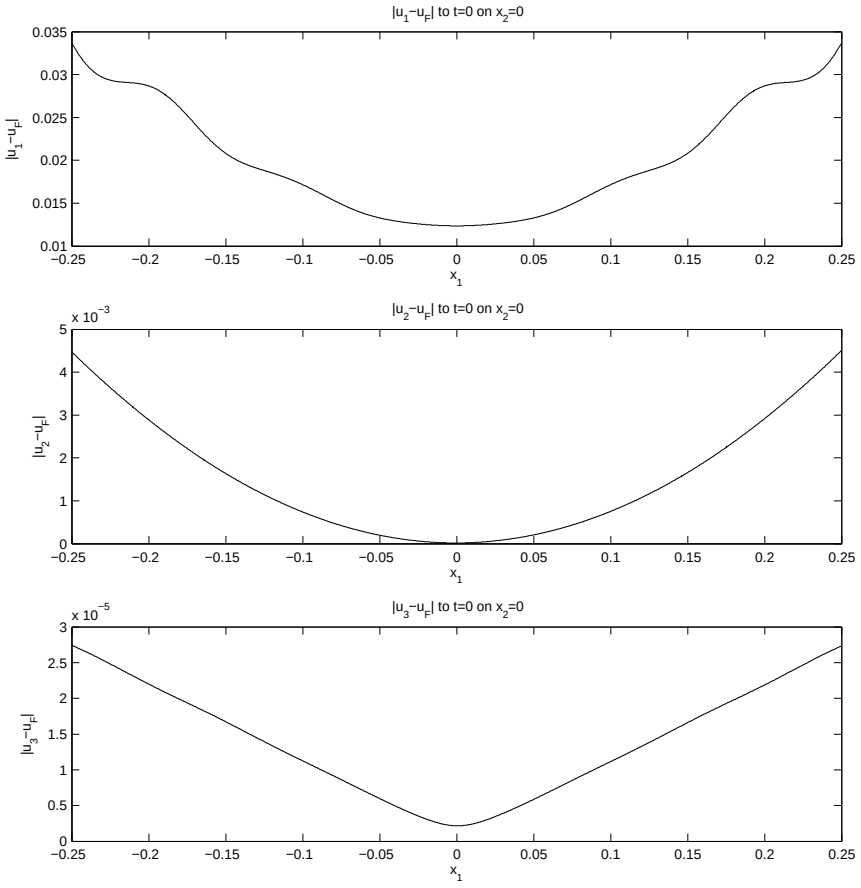

FIG. 3.2. *Differences between the Fourier transform solution and the Gaussian beam superposition solutions at* $t=0$ *for* $x_2=0$ *for the traveling waves example. Note that the scale for each graph is different.*

3.3. Initial value problem for an expanding ring of waves. We choose the initial data for the PDE (3.1) to be

$$f=u|_{t=0}=e^{ik\Phi(x)}\left[A(x)+\frac{1}{k}B(x)\right],$$

where

$$\Phi(x)=\frac{1}{2}\left(1-\sqrt{x_1^2+x_2^2}\right),$$
$$A(x)=\begin{cases}\exp\left((10(|x|-1)^2-1)^{-1}+1\right) & \text{for } 10(|x|-1)^2<1,\\ 0 & \text{otherwise,}\end{cases}$$
$$B(x)=0,$$

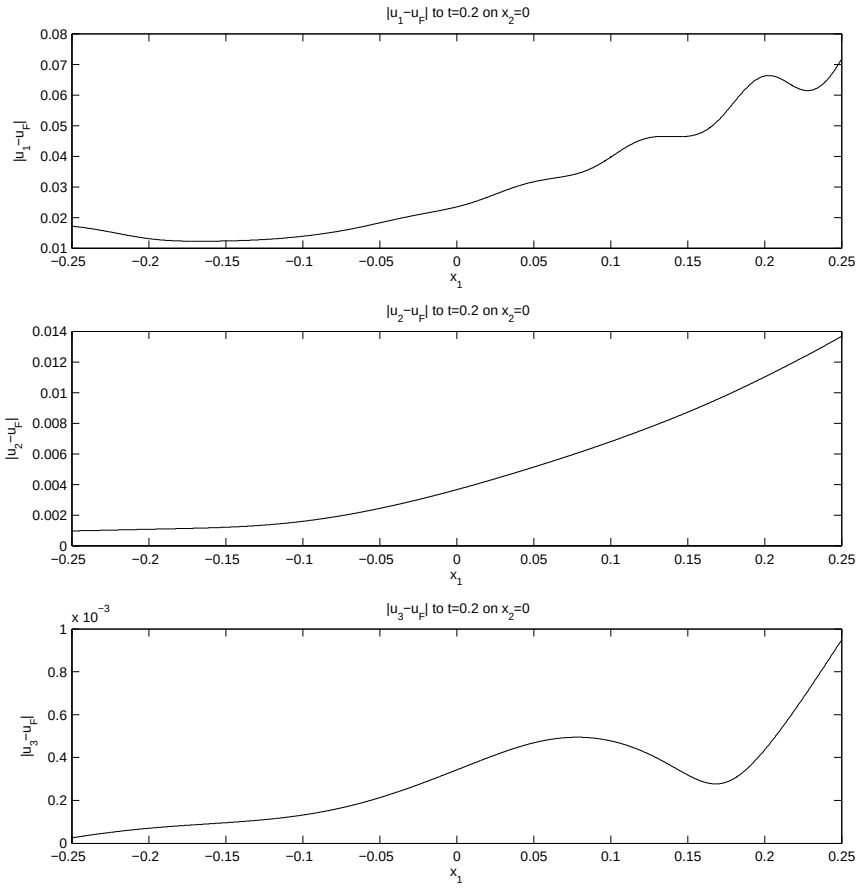

FIG. 3.3. *Differences between the Fourier transform solution and the Gaussian beam superposition solutions at* $t=0.2$ *for* $x_2=0$ *for the traveling waves example.*

and

$$g=u_t|_{t=0}=e^{ik\Phi}\left[ik\Phi_t\left(A+\frac{1}{k}B\right)+A_t+\frac{1}{k}B_t\right],$$

where Φ_t, A_t and B_t are determined by the equations in Section 3.1 to give an expanding ring of waves. This amounts to taking the positive square root in Equation (3.5). We also fix the high frequency parameter $k=500$.

Figure 3.5 shows a set of characteristics with $|y|=1$ for $\mathcal{T}=0$ to 6 for the expanding ring of waves example. Note that the characteristics are spreading apart quickly.

Comparisons. The numerical calculations of the Fourier transform solution and the Gaussian beam superpositions were carried out using a combination of Matlab and C. The Fourier transform solution will be used as the "true" solution to find the error in the wave field that is present in the Gaussian beam superpositions. For 2^{nd} and 3^{rd} order beams, the required cut-off function ρ is obtained by mollifying the characteristic function of the set where the quadratic imaginary part of the phase is twice the rest of the imaginary part.

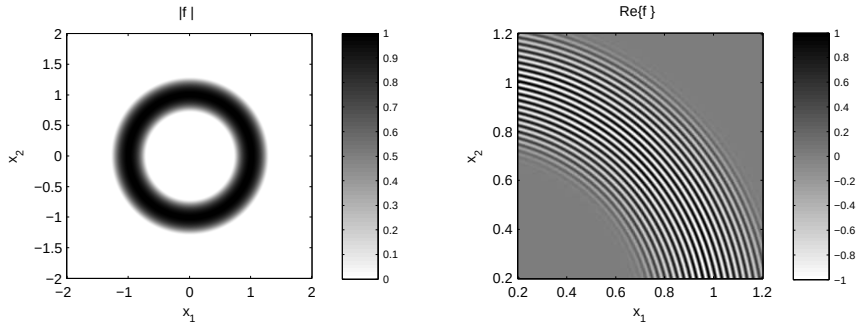

FIG. 3.4. *Initial data for the wave equation: ring of expanding waves.*

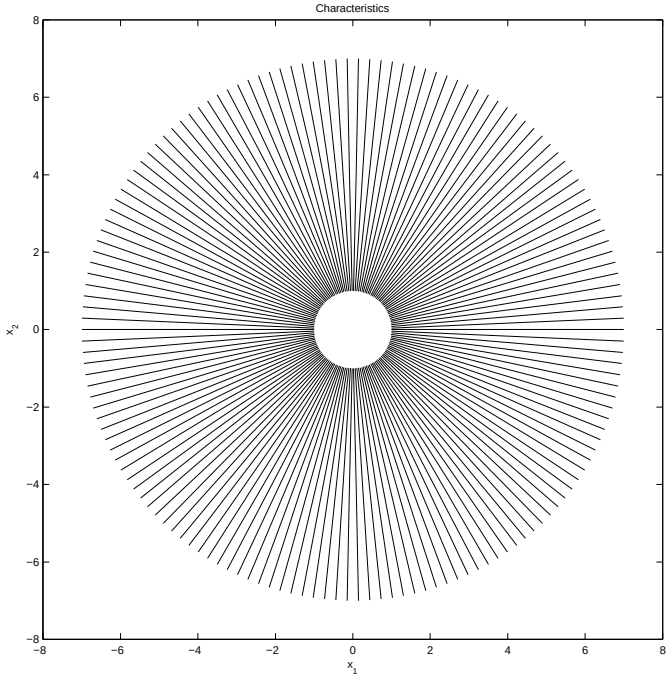

FIG. 3.5. *A set of characteristics for the wave equation for an expanding ring of waves.*

Figure 3.6 shows the absolute value of the difference between the Fourier transform solution and the Gaussian beam superpositions along $x_2 = 0$ at $t = 0$, while Figure 3.7 shows the same difference at $t = 2$. Note that the places where the error is highest correspond to the places where the amplitude has the largest gradient. This is in part the reason that the improvement in approximation of the initial data isn't as drastic as in the previous example. The numerically computed norms of the differences are given in Table 3.2.

Ray Divergence. As shown in Figure 3.5, for this particular initial data, the rays diverge quickly as time increases. However, since the accuracy of the Gaussian

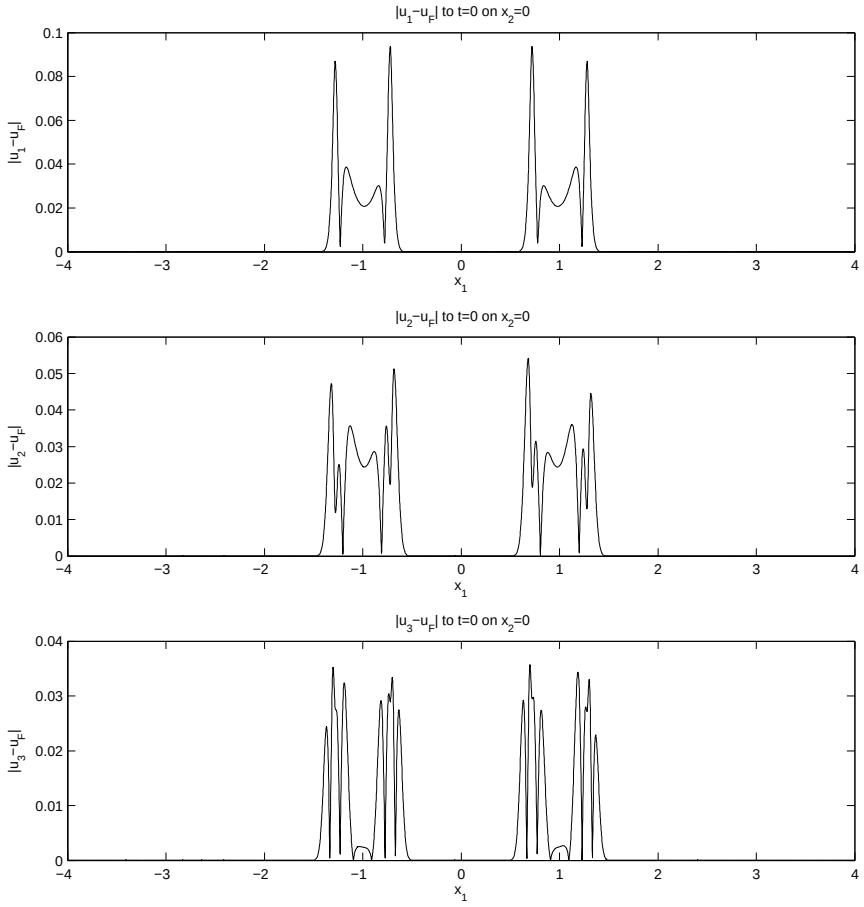

FIG. 3.6. *Differences between the Fourier transform solution and the Gaussian beam superposition solutions at $t=0$ for $x_2=0$ for the expanding ring of waves example. Note that the scale for each graph is different.*

	Difference at $t=0$		Difference at $t=2$	
	L_2-norm	H_1-norm	L_2-norm	H_1-norm
1^{st} order	0.081451	19.7417	0.085706	20.3478
2^{nd} order	0.062182	15.0985	0.064387	15.8550
3^{rd} order	0.043014	10.4802	0.046284	11.7977

TABLE 3.2. *Norm differences between the Fourier transform solution and the Gaussian beam superpositions for the expanding ring of waves example.*

beam superposition depends on how well the initial data is resolved and how accurate the individual Gaussian beams are as solutions of the wave equation, the individual Gaussian beams interfere in just the right way to maintain an accurate solution. In other words, the Gaussian beams stretch in the direction in which the rays are diverging to fill in regions of low ray density (see Figure 3.8). We can see the result

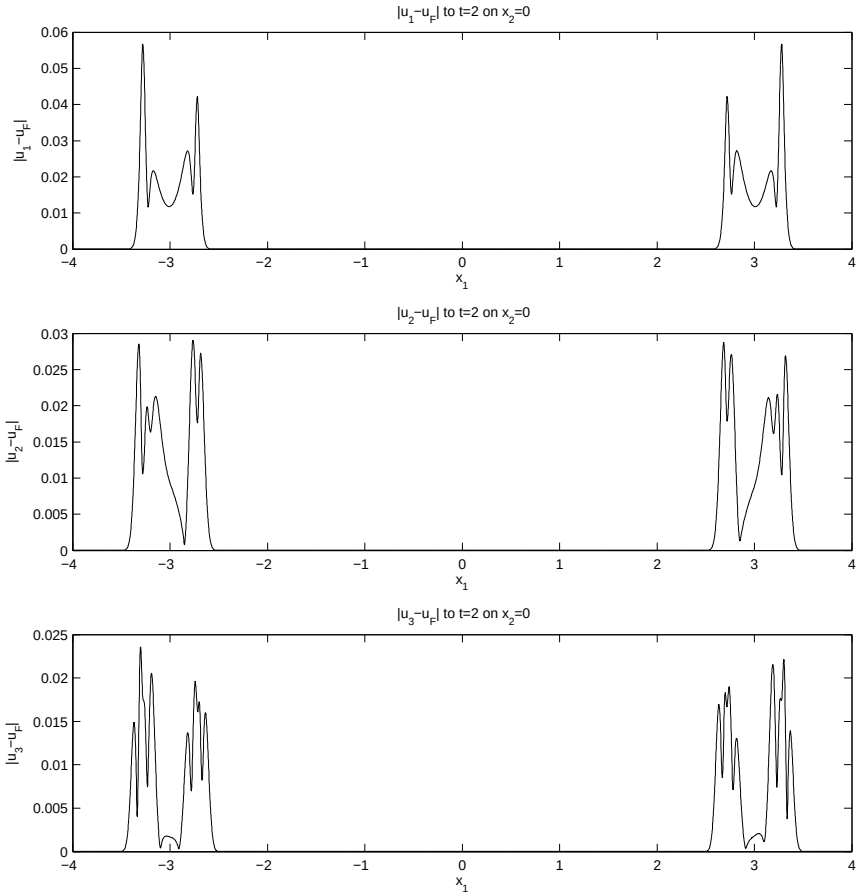

FIG. 3.7. *Differences between the Fourier transform solution and the Gaussian beam superposition solutions at* $t=2$ *for* $x_2=0$ *for the expanding ring of waves example.*

of this in Figure 3.9. While the beam centers are fairly far apart, they still provide an accurate solution.

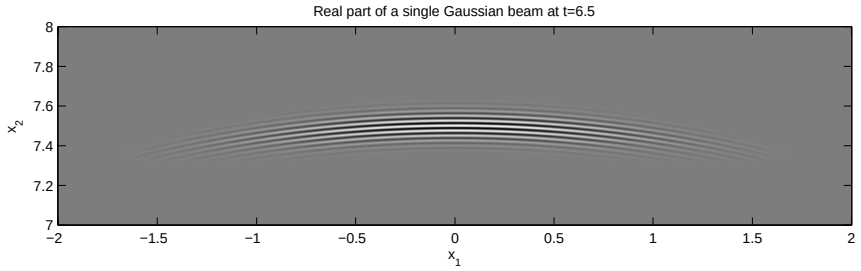

FIG. 3.8. *Real part of a single* 3^{rd} *order Gaussian beam at* $t=6.5$ *for the expanding ring of waves example.*

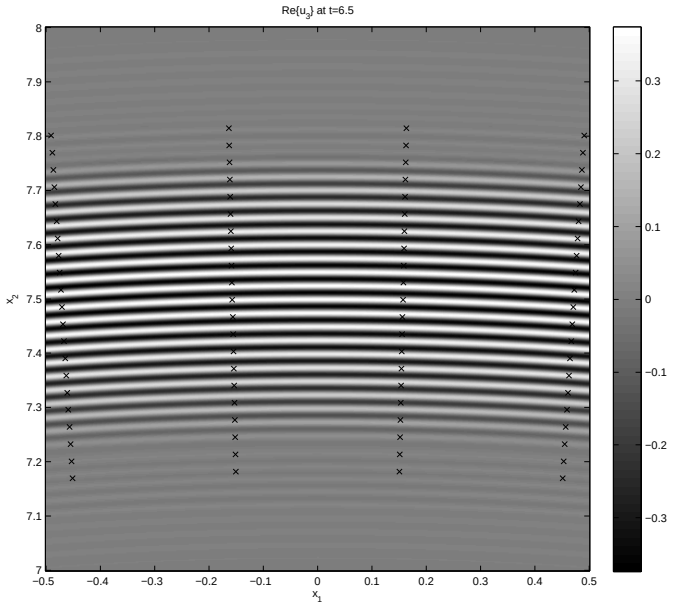

FIG. 3.9. *Real part of u_3 at $t=6.5$ and the locations of the centers of the Gaussian beams used to construct the solution (marked by '$\times$') for the expanding ring of waves example. Notice that they are quite far apart.*

3.4. Caustics. We consider an initial value problem for the constant coefficient wave Equation (3.1) that exemplifies the strength of Gaussian beam superpositions. Let the initial data be given by

$$f(x) = e^{-100|x|^2 + ik(-x_1 + x_2^2)},$$

so that the initial phase and amplitude are

$$\Phi(x) = -x_1 + x_2^2$$

and

$$A(x) = e^{-100|x|^2}.$$

The initial data for the time derivative of u, g is taken to give waves that propagate to the right. Since we are still working with the constant coefficient wave equation, the characteristics are straight lines. However, the phase is chosen in such a way so that the characteristics cross. Examining the initial data, we see that the equations for the characteristics (3.7) give:

$$\begin{aligned} \mathcal{T} &= 2s\sqrt{1+4y_2^2}, \\ \mathcal{X}_1 &= 2s + y_1, \\ \mathcal{X}_2 &= -4y_2 s + y_2. \end{aligned}$$

The solution to the wave equation will exhibit a caustic where (s, y_1, y_2) cannot be solved for in terms of $(\mathcal{T}, \mathcal{X}_1, \mathcal{X}_2)$, in other words, in places where the determinant of

the Jacobian matrix of the transformation,

$$\left|\begin{pmatrix} 2\sqrt{1+4y_2^2} & 0 & \frac{8sy_2}{\sqrt{1+4y_2^2}} \\ 2 & 1 & 0 \\ -4y_2 & 0 & 1-4s \end{pmatrix}\right|$$
$$=2\sqrt{1+4y_2^2}(1-4s)-\frac{8sy_2}{\sqrt{1+4y_2^2}}(-4y_2)$$

vanishes. Setting this expression equal to 0, we get

$$\begin{aligned} 0&=2\sqrt{1+4y_2^2}(1-4s)+\frac{32sy_2^2}{\sqrt{1+4y_2^2}},\\ 0&=(1+4y_2^2)(1-4s)+16sy_2^2,\\ 0&=1-4s+4y_2^2. \end{aligned}$$

In space-time coordinates, $(\mathcal{T},\mathcal{X}_1,\mathcal{X}_2)$, this surface is given parametrically for $p\in[1/4,\infty)$, $q\in(-\infty,\infty)$ by

$$\begin{aligned} \mathcal{T}&=4p^{3/2},\\ \mathcal{X}_1&=2p+q,\\ \mathcal{X}_2&=\pm(4p-1)^{3/2}. \end{aligned} \tag{3.10}$$

Since this is not a smooth surface, the solution to the wave equation develops a cusp caustic (see Figure 3.10).

The equations for the various Taylor coefficients that are needed to form Gaussian beams of first, second and third order are the same as in the previous section. Their superpositions are formed as before as well.

3.4.1. Numerical calculations in the presence of caustics. Since the characteristics converge towards the x_2 axis, the (x_1,x_2) support of the solution is compressed in the x_2 direction at the caustic and then it spreads apart once the rays have passed through the caustic (see Figure 3.11). The time series shown in Figure 3.11 is for a solution of the wave equation generated using a superposition of third order Gaussian beams. Note that since this solution is a superposition of Gaussian beams, it provides an accurate solution before, at and after the cusp caustic (at time $t=.5$). In fact, as can be seen from equations (3.10), after time $t=.5$ the solution is continuously passing through a caustic.

For the numerical calculations, a superposition of third order Gaussian beams is used to form the solution with $k=10^4$. The superposition integral (3.9) is discretized using a 43 by 43 grid on $[-.2,.2]\times[-.2,.2]$, and the magnitude of the solution $|u|$ is evaluated on $[-.2,1.2]\times[-.2,.2]$ using 1401×401 grid points.

3.4.2. Order of magnitude of wave amplitude at cusp caustic. Maslov theory predicts that the order of magnitude of the solution to the wave equation at a cusp caustic is $O(k^{1/4})$ as $k\to\infty$. For a discussion of the asymptotic behavior of the solution, we refer the reader to [10], Chapter 6, and for a systematic classification of several types of caustics to Chapter 7, Section 9, of [2]. To verify this behavior numerically, we evaluate the Gaussian beam superposition at the tip of the caustic for several values of the large frequency parameter k. The superposition integral (3.9) is discretized on a parabolic grid centered about (0,0). That is, the grid points are

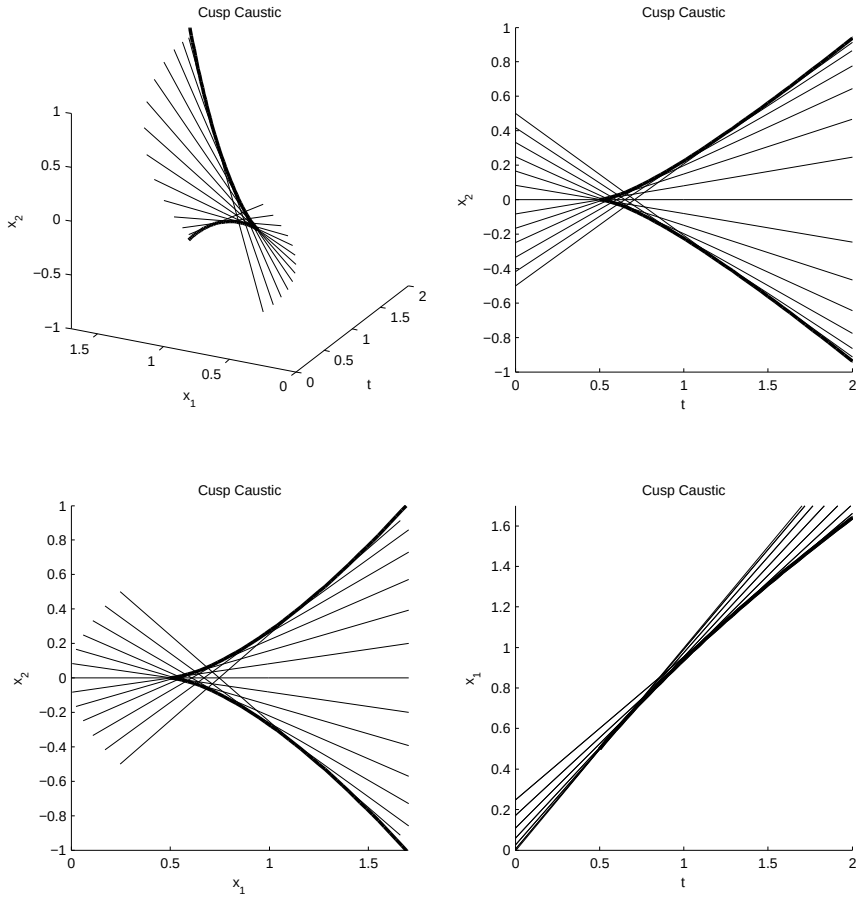

FIG. 3.10. *A set of rays that form a cusp caustic. The bold line shows the caustic set that is enveloped by this particular set of rays, which are shown by the gray lines.*

located on the family of curves $y_1 = y_2^2 + c$. For the discretization in the y_2 direction, the interval $[-.2,.2]$ is discretized using an equispaced grid. The y_1 direction is discretized using the same distance between grid points as in the y_2 direction with 9 nodes. The exact numerical values used for the discretization are given in Table 3.3. The parabolic grid is used to minimize the calculation time, and Gaussian beams that don't contribute to the solution magnitude are left out of the summation for the same reason.

A comparison between the theoretical asymptotic behavior of the magnitude of the solution and experimental results is shown is Figure 3.12. Note that the larger difference at the lower frequencies does not necessarily mean that the Gaussian beam superposition is providing an erroneous result. The Maslov prediction is an asymptotic one, so it may not be valid at the lower frequencies.

4. Conclusion

We have shown that integral superpositions of Gaussian beams can be used to approximate the initial data for PDE. Thus, through the well-posedness of the PDE, the

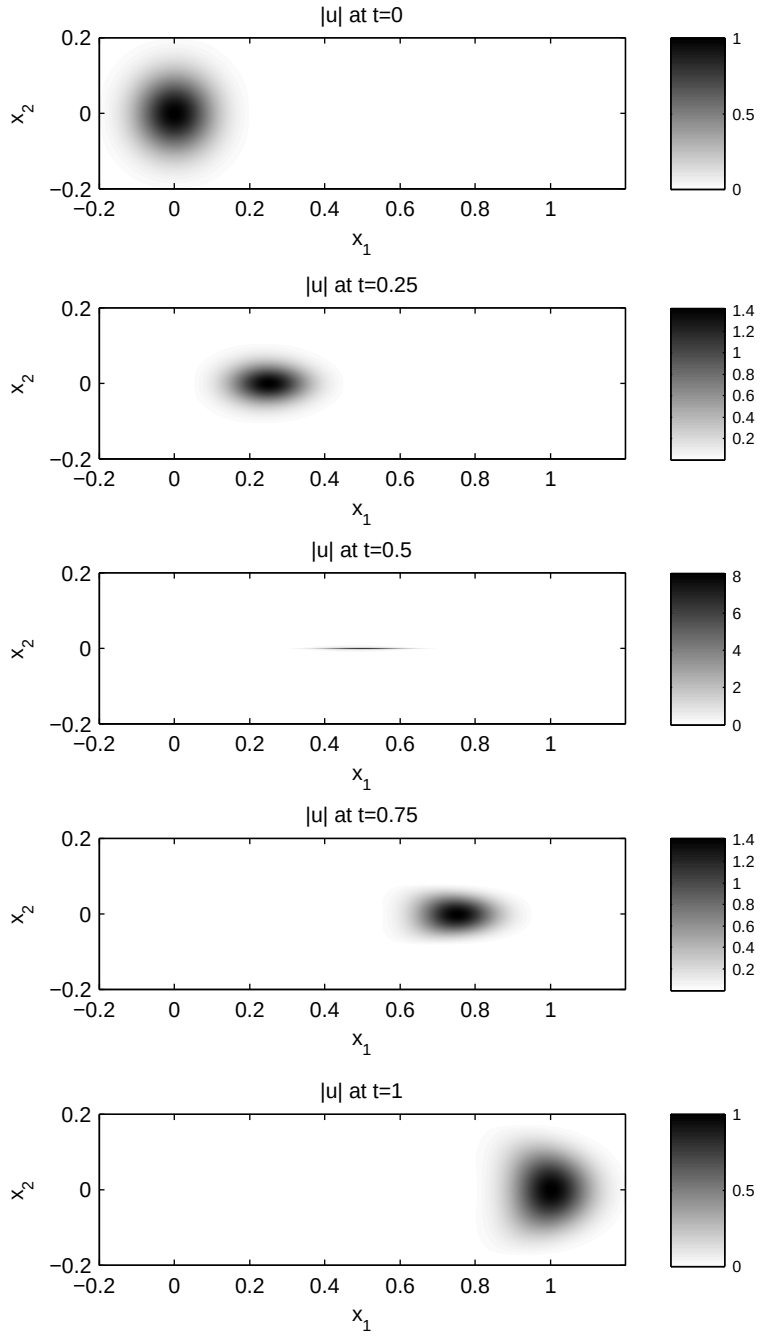

FIG. 3.11. *Time series of a solution of the wave equation with localized waves passing through a cusp caustic. Solution was computed using a superposition of third order Gaussian Beams.*

k	y_2 Nodes	$\|u\|$	k	y_2 Nodes	$\|u\|$
1,000	13	3.2211	375,000	253	24.3562
1,250	15	3.5473	500,000	291	26.3072
2,500	21	4.7616	625,000	325	27.9141
3,750	27	5.6188	750,000	357	29.2916
5,000	31	6.2964	875,000	385	30.5038
6,250	33	6.8577	1,000,000	413	31.5905
7,500	37	7.3406	1,250,000	461	33.4858
8,750	39	7.7667	2,500,000	651	40.0677
10,000	43	8.1484	3,750,000	797	44.4634
12,500	47	8.8135	5,000,000	921	47.8569
25,000	65	11.1066	6,250,000	1,029	50.6588
37,500	81	12.6194	7,500,000	1,127	53.0648
50,000	93	13.7773	8,750,000	1,217	55.1849
62,500	103	14.7272	10,000,000	1,301	57.0876
75,000	113	15.5388	12,500,000	1,455	60.4102
87,500	123	16.2510	25,000,000	2,057	71.9804
100,000	131	16.8882	37,500,000	2,519	79.7282
125,000	147	17.9965	50,000,000	2,907	85.7177
250,000	207	21.8198			

TABLE 3.3. *Details of the discretization used to obtain the magnitude of the wave equation solution at a cusp caustic.*

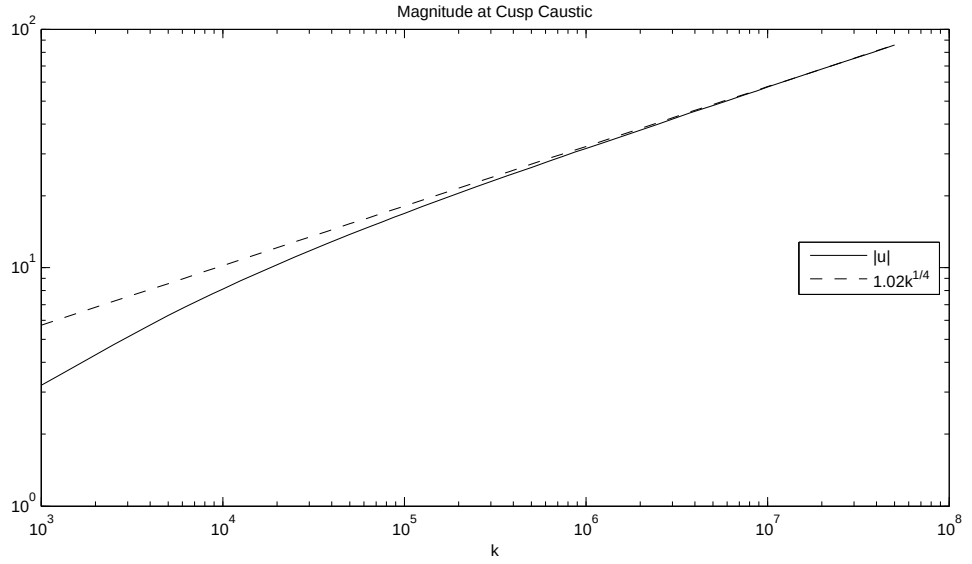

FIG. 3.12. *Comparison of the solution magnitude at a cusp caustic with Maslov theory prediction. Maslov theory predicts that* $|u| = O(k^{1/4})$. *This behavior is present in the Gaussian beam superposition solution.*

integral superposition gives an approximate solution. In particular, we have proved a well-posedness estimate for the wave equation and used a Gaussian beam superposition to approximate the solution to the 2-D wave equation for an expanding ring of waves. The Gaussian beams in this particular case stretch to fill in the gaps that result due to the divergence in the rays. In traditional geometric optics methods, one would need to insert more rays to resolve the wave field in such places. Since this is not necessary in the presented method, this example shows the power of the Gaussian beam method.

Another advantage of the Gaussian beam method is that the obtained solution is global. This means that even in the presence of caustics the Gaussian beam solution is valid, before, after and at the caustic region. As an example, we have computed the order of magnitude of the solution at a cusp caustic as a function of the high frequency parameter and compared it to the asymptotic behavior predicted by Maslov theory. While in geometric optics methods the solution can be extended past caustics by using a phase correction, a computation of the solution at a caustic is not possible. The identification of caustics and their corrections are non-trivial in standard geometric optics. Using Gaussian beams, one can easily compute the global wave field.

REFERENCES

[1] V. Červený, M. Popov and I. Pšenčík, *Computation of wave fields in inhomogeneous media — Gaussian beam approach*, Geophys. J. R. Astr. Soc., 70, 109–128, 1982.

[2] V. Guillemin and S. Sternberg, *Geometric Asymptotics*, Mathematical Survey and Monographs, American Mathematical Society, 14, 1977.

[3] N.R. Hill, *Prestack Gaussian-beam depth migration*, Geophysics, 66, 1240–1250, 2001.

[4] L. Hörmander, *On the existence and the regularity of solutions of linear pseudo-differential equations*, L'Enseignement Mathématique, XVII, 99–163, 1971.

[5] L. Klimeš, *Expansion of a high-frequency time-harmonic wavefield given on an initial surface into Gaussian beams*, Geophys. J.R. Astr. Soc., 79, 105–118, 1984.

[6] L. Klimeš, *Discretization error for the superposition of Gaussian beams*, Geophys. J.R. Astr. Soc., 86, 531–551, 1986.

[7] S. Leung, J. Qian and R. Burridge, *Eulerian Gaussian beams for high frequency wave propagation*, Geophysics, 72, SM61–SM76, 2007.

[8] J. Ralston, *Gaussian beams and the propagation of singularities*, Sudies in PDE, Stud. Math., 23, 206–248, 1982.

[9] N.M. Tanushev, J. Qian and J.V. Ralston, *Mountain waves and Gaussian beams*, SIAM Multiscale Modeling and Simulation, 6, 688–709, 2007.

[10] M.E. Taylor, *Partial Differential Equations I: Basic Theory*, Appl. Math. Sci., Springer-Verlag, 115, 1996.